Complementary studies of $T = 2$ ^{30}Al and the systematics of intruder states

T. A. Hinners, Vandana Tripathi, S. L. Tabor, A. Volya, P. C. Bender, C. R. Hoffman, Sangjin Lee, and M. Perry
Department of Physics, Florida State University, Tallahassee, Florida 32306, USA

P. F. Mantica, A. D. Davies, S. N. Liddick, W. F. Mueller, A. Stolz, and B. E. Tomlin
National Superconducting Accelerator Laboratory, Michigan State University, East Lansing, Michigan 48824, USA

(Received 17 September 2007; published 13 March 2008)

Low-spin states were studied in ^{30}Al following the β decay of ^{30}Mg produced in the fragmentation of 140-MeV/AMU ^{48}Ca. Analysis of the β-γ and β-γ-γ coincidences revealed a new 1^+ state at 2413 keV, confirmation of the level scheme, and a more accurate half-life measurement of 315(6) ms for the ^{30}Mg ground state. Higher-spin states were investigated in the reaction of ^{14}C on ^{18}O at 22 MeV. Protons and deuterons were detected in a segmented E-ΔE Si telescope in coincidence with one or two γ rays in the FSU Ge detector array. A comparison of the resulting level and decay scheme with predictions of the *sd* shell model shows good agreement with all but six of the states in both excitation energy and γ-decay branching ratios. The root-mean-square deviations in energy of these states using the older USD and newer USDA and USDB interactions were 265, 176, and 173 keV, respectively. The remaining six states are well described as 4^- to 7^- states, similar in relative energy to those in ^{28}Al but shifted down by about 1200 keV. These states also agree well with the predictions of shell-model calculations using the WBP interaction. A comparison of the lowest 4^- states in even A Na, Al, and P isotopes shows a systematic decrease in energy with increasing N and with decreasing Z. The energies of the 4^- states are almost identical in nuclei with the same N-Z values.

DOI: 10.1103/PhysRevC.77.034305 PACS number(s): 27.30.+t, 23.20.Lv, 23.20.En, 21.60.Cs

I. INTRODUCTION

The existence of intruder states at high excitation energies based on configurations involving orbitals outside the shell being filled comes as no surprise. However, their presence at low excitations and even in the ground states (g.s.) of neutron-rich nuclei has been surprising at times and continues to challenge theoretical understanding. One of the early surprises was the unexpected $\frac{1}{2}^+$ ground states of ^{11}Be [1] when the seventh neutron is expected to occupy the $p_{1/2}$ orbital. Figure 1 in Ref. [1] illustrates another important characteristic, namely the fact that the position of the neutron intruder state depends not only on the number of neutrons but also on the number of protons. The position of the $\frac{1}{2}^+$ intruder state falls with decreasing Z even for constant N.

For the normal states, the demonstration that one effective interaction with smooth A dependence (USD) [2,3] can describe most of the structure observed in the *sd* shell was one of the early successes of the large-basis shell model. Because the interaction was fitted to the known states throughout the shell, it may include some of the effects of two-particle-two-hole intruder configurations. The failures of a model can be as instructive as its successes. The failure to reproduce the ground-state binding energy of ^{31}Na, although giving excellent agreement for the lighter isotopes [4], was an early indication for intruder configurations in the ground state of some *sd*-shell nuclei that are not well reproduced by calculations employing the USD effective interaction. This region of nuclei with Z near the bottom of the *sd* shell and N near the top, where the energies of intruder-dominated configurations fall below those of the normal configurations, has been called the "island of inversion." Recent studies have traced out the decreasing energies of intruder configurations with increasing N in the Na isotopes [5–7].

Recently new *sd* effective interactions (USDA and USDB) have been derived by fitting the greatly expanded structure now known in *sd*-shell nuclei [8]. Even though considerably more levels in neutron-rich nuclei were included in adjusting the new interactions, the underprediction of the binding energies of nuclei in the island of inversion remains. Inversion effects are reasonably accounted for in calculations, including the *fp* shell, e.g., by using the SDPF-M interaction that involves a Z- and N-dependent shell gap [9].

The present work on ^{30}Al was initiated to see whether the newer *sd* effective interactions provide a better description of a neutron-rich nucleus not involved in the adjustment and to provide further information on the behavior of intruder structures as a function of N and Z approaching the island of inversion. Complementary approaches were used: Low-spin states were explored following the β decay of the 0^+ ground state of ^{30}Mg produced in the fragmentation of ^{48}Ca, and high-spin states were investigated by detecting particle-γ coincidences in a heavy-ion reaction involving a long-lived radioactive beam.

Excited states were previously observed in ^{30}Al in the ^{30}Si(t,^{3}He) reaction [10–12], following the β decay of ^{30}Mg [13,14] and in a particle-γ coincidence experiment with the ^{14}C(^{18}O,pn) reaction [15]. An early suggestion that the first excited state is isomeric was ruled out by subsequent work. Also a tentative state at 1000(30) keV [10] or 991 keV [15] was not seen in other experiments and will be discussed in this article.

II. EXPERIMENTAL DETAILS

A. β decay

In the experiment to study the β decay of ^{30}Mg, a ^{48}Ca beam was used to produce the parent nucleus, ^{30}Mg, by intermediate-

energy projectile fragmentation at the National Superconducting Cyclotron Laboratory (NSCL) at Michigan State University. The ^{48}Ca beam was accelerated to 140 MeV/A using the coupled cyclotron facility. The desired $^{48}Ca^{20+}$, with a maximum beam current of 15 pnA, was then fragmented in a 700-mg/cm^2-thick ^{9}Be target located at the object position of the fragment separator, the A1900, to obtain the ^{30}Mg parent nuclei. A 300 mg/cm^2 wedge-shaped Al degrader was used in conjunction with the A1900 to disperse the fragments according to their mass-to-charge ratios. A "cocktail" secondary beam consisting of F, Ne, Na, and Mg isotopes was selected.

These fragments were then implanted in the double sided silicon micro-strip detector (DSSD), which forms part of the beta counting station (BCS) [16]. The DSSD was used to determine the location and time of each implantation and subsequent β decay. A 10-mm Al degrader was placed in front of the DSSD to ensure the complete implantation within the 985-μm-thick DSSD. Energy loss and time-of-flight information were used to separate the different species reaching the DSSD. A plot of the time-of-flight vs. dE can be seen in Fig. 1 of Ref. [17], where the various nuclei reaching the DSSD are distinctly separated. Each implantation and decay event was recorded and tagged with an absolute time stamp generated by a free-running clock (30.5-μs repetition rate).

Fragment-β correlations were established in software, where a low-energy β event was correlated to a high-energy implantation in the same pixel of the DSSD. Light particles, transmitted along with the secondary beam, were vetoed by a scintillator placed at the end of the BCS for the purpose of increasing the fragment-β correlation efficiency. To generate a decay curve, the differences between the absolute time stamp of the correlated β events and implant events were histogrammed. Implantation events were rejected if not followed by a β event within a certain time period in the same pixel or if a second implantation occured before a β decay. This was used to enhance background supression. A 3.6-s time period was selected for analyzing the β-delayed γ transitions in ^{30}Al, whereas a 10-s time period was used to generate the decay curve.

The β-delayed γ rays were detected using 12 detectors of the segmented germanium array (SeGA) [18] arranged around the BCS. Each detector is composed of an 8-cm-long by 7-cm-diameter Ge crystal divided into eight 1-cm-wide segments along the crystal length and four quadrants on the crystal face. The Ge detectors were energy and efficiency calibrated using standard calibration sources. The measured peak detection efficiency was ~5% at 1 MeV.

B. In beam

Excited states in ^{30}Al were populated through the ^{18}O(^{14}C, $pn\gamma$) reaction at a beam energy of 22 MeV provided by the Florida State University Tandem Accelerator. The ^{18}O target with a thickness of 200 μg/cm^2 was made by anodizing Ta in an electrolytic cell with water enriched to 85% in ^{18}O on an 0.0127-mm-thick Ta backing. The charged particles from the reaction were detected in the FSU E-ΔE silicon particle telescope. This telescope consisted of three annularly segmented silicon surface barrier detectors. A 150-μm-thick silicon detector was used for the ΔE detector, and the two silicon detectors with thicknesses of 1500 μm each were combined to form the E detector. A more detailed description of the E-ΔE telescope setup can be found in Ref. [19].

Following the charged-particle decay, the γ radiation was detected by the FSU Compton suppressed high-purity germanium (HPGe) detector array. At the time of this experiment, the array consisted of three four-crystal Clover detectors and six single crystal detectors. The three Clover detectors were located at 90° from the beam axis along with two single crystal detectors. In addition, two single crystal detectors were each located at 35° and 145° relative to the beam. The minimum trigger condition was a signal in one of the E detectors and another in a γ detector within the resolving time of about 70 ns. The data were written to disk during the experiment and later sorted into matrices for data analysis using GNUSCOPE [19]. In playback, the ^{30}Al events were selected by requiring the detection of a p or d in the particle telescope through gates drawn in the E-ΔE plane in coincidence with one or two γ rays. The dimensions of the particle-γ and particle-gated γ-γ matrices were 4000 × 4000, with a dispersion of 2 keV/channel. The matrices gated on p and d events were added together to combine both the p-n and d exit channels to improve the statistics.

Angular distributions were measured by comparing the intensities of γ lines in the 90° detectors with those in the combined 135° and 45° detectors. The relative normalization between the two spectra was determined by fitting the 2235 keV $2^+ \rightarrow 0^+$ $E2$ transition in ^{30}Si that must have a zero mixing ratio. The Clover detectors were treated in self-suppression mode just for the angular distribution measurements so that the normalization would be approximately energy independent. The angular distribution attenuation coefficients were calculated based on an average geometry for the detectors. A Gaussian distribution of magnetic substates was assumed with a width $\sigma = 0.5\hbar$ based on fits to known transitions in other nuclei in the data set.

III. RESULTS

A. β decay

1. Half-life measurement

The decay curve for ^{30}Mg was created by histogramming the time differences between the identified ^{30}Mg implants and β decay events in the same pixel for time intervals up to 10 s. The resulting decay curve is shown in Fig. 1 along with the fit based on the Bateman equations for the sequential decay of ^{30}Mg and ^{30}Al. The decay curve was constructed using three components, the decay of ^{30}Mg, the growth and decay of the daughter nucleus ^{30}Al, and the background. The decay constants of ^{30}Mg and the background were allowed to vary, as was the intial number of β-decaying particles. The decay curve from β's correlated with γ rays of energy 244 or 444 keV was also fitted, as shown in Fig. 2. This fit was created using a two-component exponential fit that included the parent decay and a long-lived background decay. Both decay constants for

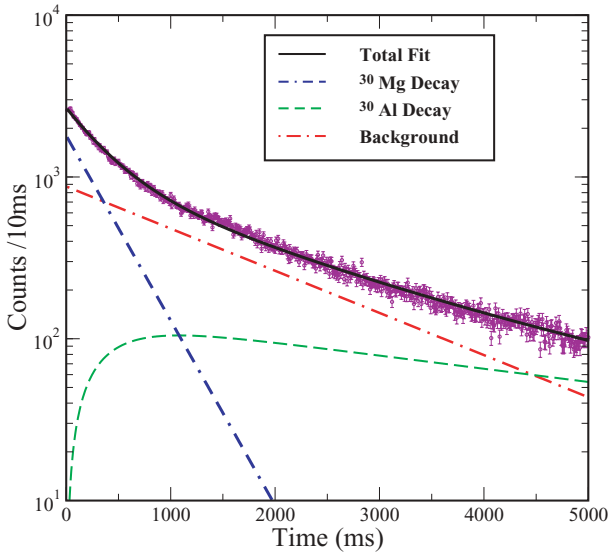

FIG. 1. (Color online) The decay curve for ^{30}Mg. Counts per 10 s vs. time (ms). The half-life was determined to be 314 ± 5 ms.

the parent and background decay were allowed to vary, as was the inital number of particles. The half-life obtained from the fragment-β correlated events was found to be 316 ± 5 ms, and that of the fragment-β-γ was calcuated to be 314 ± 7 ms. The average of these half-lives was used to determine the adopted half-life of ^{30}Mg. The value of 315 ± 6 ms is in good agreement with previous measurements of 325 ± 30 ms [13] and 340 ± 20 ms [20] and has higher precision.

2. *Level scheme*

The β-delayed γ spectrum displayed five γ lines that represent transitions in ^{30}Al. Lines at 243, 443, 685, and 2165 keV have been previously reported for ^{30}Al, but the 2165-keV line was not placed in the level scheme [13]. A new

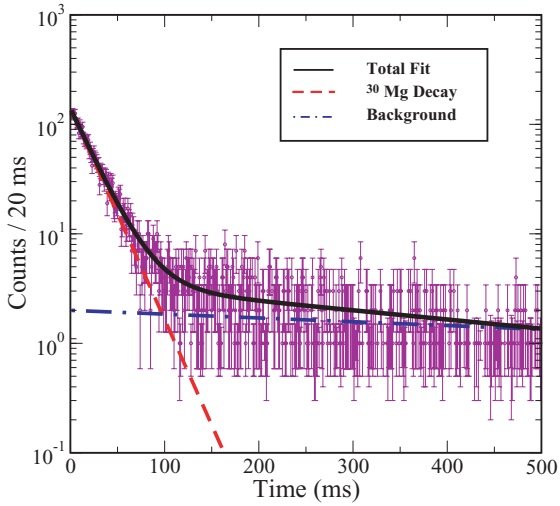

FIG. 2. (Color online) The decay curve for the combined 244- and 444-keV γ transitions. Counts per 20 ms vs. time (ms). The half-life was determined to be 312 ± 7 ms.

TABLE I. γ transitions following the β decay of ^{30}Mg.

E_γ (keV)	Intensity	Nucleus	$E_f \rightarrow E_i$ (keV)
243.9(5)	100	^{30}Al	244 → 0
443.9(5)	96(2)	^{30}Al	688 → 244
686.8(20)	2.3(3)	^{30}Al	688 → 0
1724.9(15)	6.4(8)	^{30}Al	2413 → 688
2169.8(15)	3.5(5)	^{30}Al	2413 → 244
1397.7(10)	2.9(5)	^{29}Al	1398 → 0
2236.0(10)	65(3)	^{30}Si	2236 → 0
3498.0(12)	32(5)	^{30}Si	3498 → 0

1725-keV transition was observed in this study, which along with the 2170-keV line (2165 in Ref. [13]) leads to a new state at 2413 keV. The placement of all the lines in the present β-decay work is confirmed by the β-γ-γ coincidences shown in Figs. 3 and 4. The β-decay level scheme deduced from the present work is shown in Fig. 5. The energies and intensities of the γ lines following the β decays of ^{30}Mg are listed in Table I. The nucleus in which the γ transition occurs is also listed.

The β-decay branching to each level in the daughter nucleus was calculated from the difference between γ-ray intensities feeding into and out of the level, using the measured SeGA efficiency and utilizing the initital number of β-decaying particles derived from γ transitions populating the ground state of ^{30}Si [21]. The possibility of β-delayed neutron decay was accounted for by measuring the branching to the first excited state in ^{29}Al, which was found to be approximately 2% and can be taken as a lower limit. The branching to the 244-keV state was approximately zero, suggesting that it is not populated by allowed β decay. The ground-state branch is also very small, which is consistent with the previously assigned spin and parity of 3^+. The apparent log ft values were deduced using the measured intensities for β decay, the

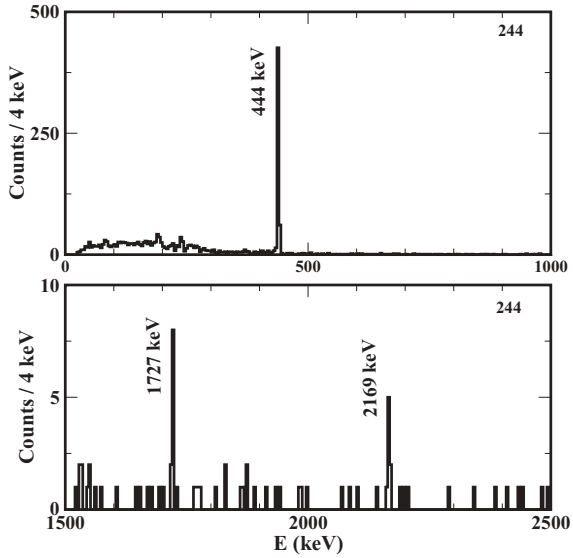

FIG. 3. Coincidences with β's from the β-decay experiment and the 244-keV line show the known 444-keV and the two new 1725- and 2170-keV γ transitions.

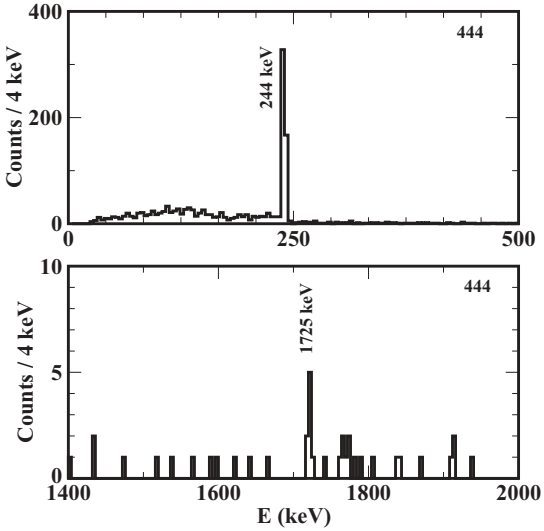

FIG. 4. Coincidences with β's from the β-decay experiment and the 444-keV line show the known 244-keV and the new 1725-keV γ transitions.

measured half-life, and the Q_β values from the literature [22]. The apparent log ft values for the 688 and 2413 keV states are 3.8 ± 0.5 and 4.1 ± 0.4, respectively. These clearly represent allowed β-decay from the 0^+ ground state of ^{30}Mg and confirm the previous 1^+ assignment to the former state [13] and provide a new 1^+ assignment to the latter.

B. In beam

Analysis of data from the ^{18}O(^{14}C,$pn\gamma$)^{30}Al reaction yielded many new transitions not observed in β decay or previous work. These transitions were observed via p-γ-γ

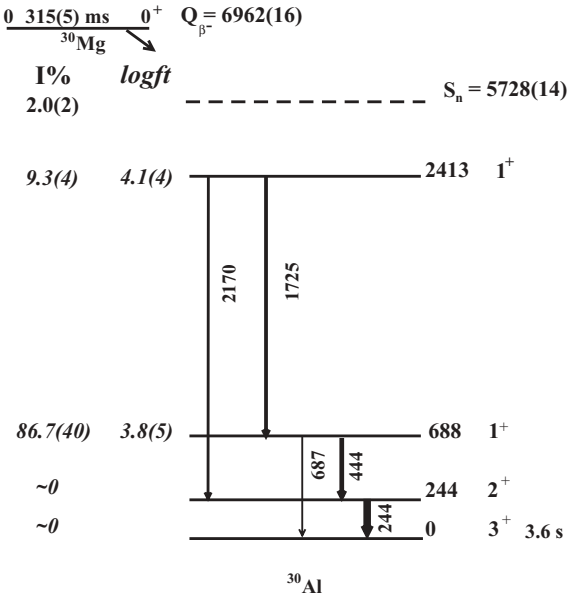

FIG. 5. The β-decay level scheme for ^{30}Al, including the two new transitions and new excited state. Transition line thickness indicates the relative intensity. All energies are in keV.

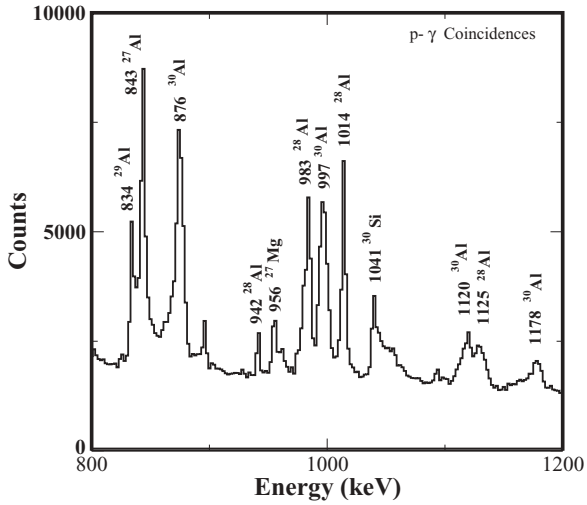

FIG. 6. The particle-γ spectrum in the region of a reported 991-keV line.

and d-γ-γ coincidences. Four of the previously known γ transitions and 13 new ones were observed. From these coincidences, the known 244-, 688-, 1120-, and 1246-keV states were confirmed. In addition, γ decays were observed from 6 states previously known only from the charge exchange experiments [11], and 4 new states were determined from their γ decays. The 991-keV γ transition reported in Ref. [15] from a proposed state at 991 keV was not seen in the present work. The particle-γ spectrum, Fig. 6, shows no evidence for a 991-keV transition. Coincidence spectra for various transitions in ^{30}Al are shown in Figs. 7, 8, 9, and 10.

The 1725-keV transition seen in the in-beam experiment must be different from the one seen in β decay because the former does not show coincidences with the 444-keV line (see Fig. 7) that appear in the later (Fig. 4). Coincidences

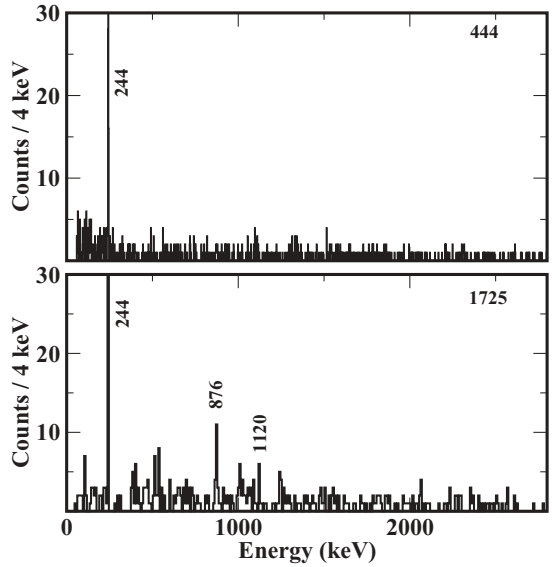

FIG. 7. Spectra from the in-beam experiment in coincidence with protons or deuterons and the 444-keV (top) or 1725-keV (bottom) lines.

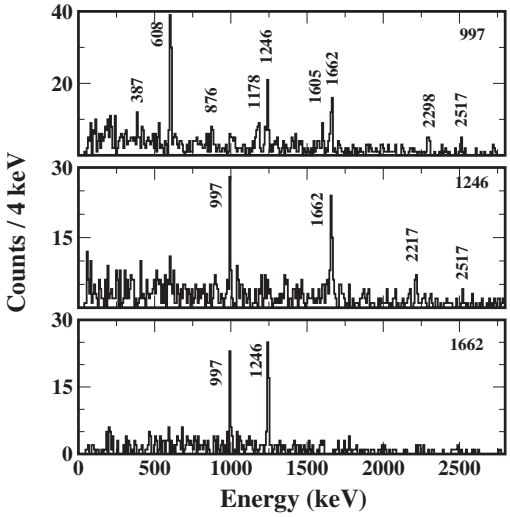

FIG. 8. Spectra from the in-beam experiment in coincidence with protons or deuterons and the 997-keV (top), 1246-keV (middle), and 1662-keV (bottom) lines.

between the 997- and 1605-keV lines (see Figs. 8 and 9) clearly establish a state at 5510 keV. The energy difference between the 3905- and 2298-keV states is 1607 keV, which is very close to that of the 5510 → 3905 keV transition. The possibility of a 1605–1607 keV doublet is also suggested by a possible peak around that energy in the 1605-keV gated coincidence spectrum (Fig. 9). The level scheme and the energies and intensities of the γ lines can be seen in Fig. 11 and Table II, respectively.

TABLE II. γ transitions observed in ^{30}Al in the in-beam experiment.

E_x (keV)	E_γ (keV)	Intensity
243.7(5)	243.7(5)	100
687.8(5)	444.1(5)	19(2)
1120.2(10)	1120.2(10)	10(2)
	875.9(9)	22(2)
1246.2(8)	1246.2(8)	60(3)
1562.2(12)	1318.5(15)	0.9(3)
1801.7(15)	1558.0(16)	1.8(5)
2298.4(12)	2298.4(10)	40(8)
	1178.3(28)	3.3(6)
2845.5(10)	1725.3(10)	17(2)
2907.7(13)	1661.5(14)	16(5)
	607.7(9)	37(5)
3463.6(12)	2217.4(15)	1.1(2)
3905.1(13)	997.4(13)	25(3)
	1605.1(25)	2(1)
4292.5(11)	387.4(10)	10(1)
5510.2(25)	1605.1(25)	8(4)
6422.1(31)	2517.0(31)	7(2)

IV. DISCUSSION

The states observed in the present experiment are compared with those reported previously in Fig. 12. There is a clear one-to-one correspondence between the present work and the older charge-exchange results [11] up through the 2298-keV level. The differences in energy are well within the 15- to 20-keV uncertainties reported for the charge exchange results. Above this, the 2413-(1^+ seen only in β decay), 2846-, 4293-, 5510-, and 6422-keV states appear to have no counterparts reported in charge exchange. Counterparts were seen for the 2908-, 3464-, and 3905-keV levels.

A. Spins

The goodness of fit χ^2 between the measured and theoretically expected angular distribution for the 244-keV transition to the 3^+ ground state [13] is graphed as a function of mixing

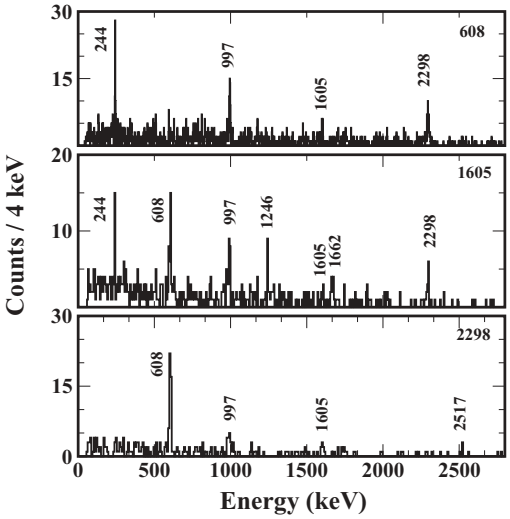

FIG. 9. Spectra from the in-beam experiment in coincidence with protons or deuterons and the 608-keV (top), 1605-keV (middle), and 2298-keV (bottom) lines.

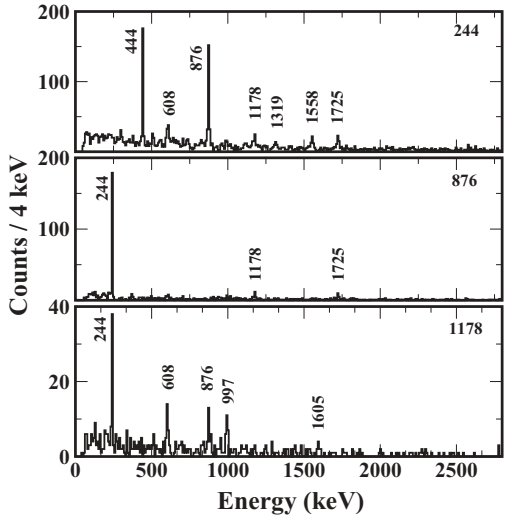

FIG. 10. Spectra from the in-beam experiment in coincidence with protons or deuterons and the 244-keV (top), 876-keV (middle), and 1178-keV (bottom) lines.

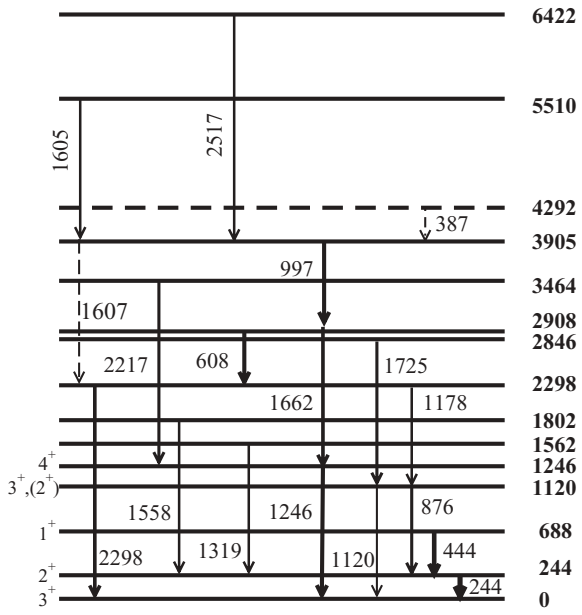

FIG. 11. Level and decay scheme from the in-beam experiment.

ratio δ for several possible spins of the 244-keV state in Fig. 13. Only a mixing ratio of $\delta = 0$ is possible for the spin-parity hypothesis of 1^+ and the fit is very poor at this point. The hypothesis of 3^+ would lead to $\delta \sim 0.62$ and an unreasonably large $E2$ admixture for such a low-energy transition. However, the hypothesis of 2^+ gives an excellent fit at $\delta = 0$ for pure $M1$ decay, which is expected for a low-energy transition. Thus, we assign 2^+ to the 244-keV state. This assignment is consistent with the nonobservation of direct β feeding from the 0^+ ground state of ^{30}Mg. The 2^+ assignment is also consistent with the tentative 1^+ or 2^+ in previous work [11,15]. Fits to the angular distribution of the 444-keV line are shown in Fig. 13. In this case, the spin and parity of the 688-keV state have already been assigned 1^+, so several spin hypotheses are shown for the 244-keV state. J^π of 2^+ implies a nearly zero mixing ratio for the 444-keV transition, in agreement with the assignment based on the 244-keV angular distribution. Hypotheses of 1^+ or 3^+ imply substantial (and therefore unlikely) $E2$ components. Note that the existence of the 444-keV transition from a 1^+ state rules out any spin above $3\hbar$ for the 244-keV state.

Fits to the angular distribution of the 876-keV line (Fig. 13) rule out pure $E2$ decay and therefore, spins of 0^+ or 4^+, for the 1120-keV state. Possible spins of 1, 2, or 3 give good fits. The choice of 3^+ implies the smallest mixing ratio, but the possibility of significant $E2$ admixtures increases with the square of the transition energy and cannot be ruled out for the 876-keV decay. Spins of 2 or 3^+ were assigned to the 1120-keV state in the charge exchange experiment, with the former spin favored [11]. However, in a reanalysis of this data, only a spin of 3 was indicated in Fig. 3 of Ref. [12]. This is consistent with the preference for 3^+ in the present work. Fits to the 1246-keV transition (Fig. 13) favor spins of 2^+ or 4^+ for the 1246-keV state, with 4^+ giving a nearly zero mixing ratio. 1^+ and 3^+ are ruled out, but 5^+ is also possible. The fact that the 1246-keV state decays only to the 3^+ ground state and not to the 2^+ or 1^+ states suggests a higher spin. Altogether,

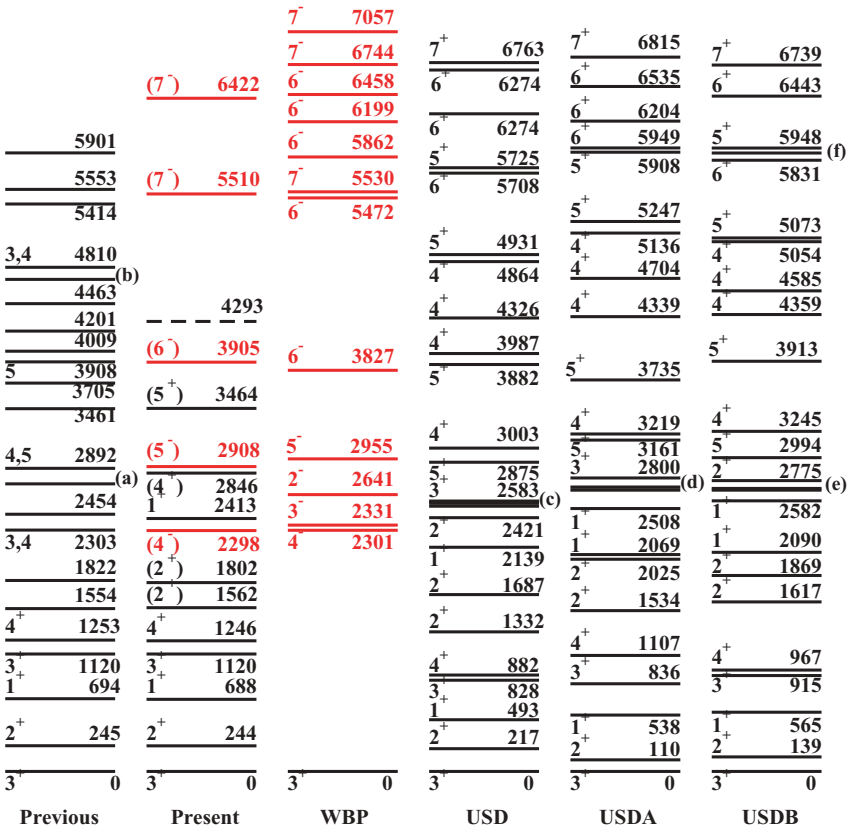

FIG. 12. (Color online) A comparison of the present results with previous experimental work and shell-model calculations using the WBP, USD, USDA, and USDB interactions. Not all the predicted lower-spin states are shown above 2 MeV to reduce clutter in the figure. Levels not labeled in the figure for lack of space are (a) 2744 keV (no spin-parity/assignment) (b) 4694 keV (no spin-parity/assignment) (c) 2538 1^+ and 2560 4^+keV, (d) 2684 keV 2^+ and 2714 keV 4^+, (e) 2646 keV 4^+ and 2679 3^+, and (f) 5891 keV 5^+. As discussed in the text, the WBP results were shifted down by about 1 MeV.

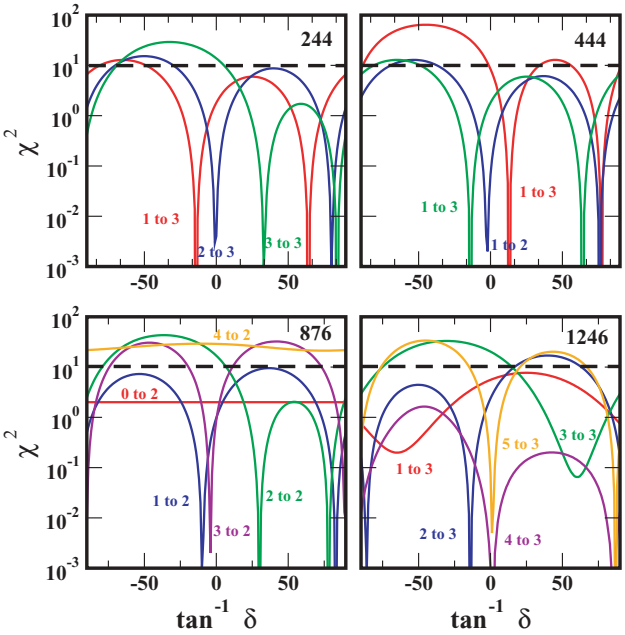

FIG. 13. (Color online) Goodness of fit χ^2 as a function of mixing ratio δ for the 244-, 444-, 876-, and 1246-keV transitions.

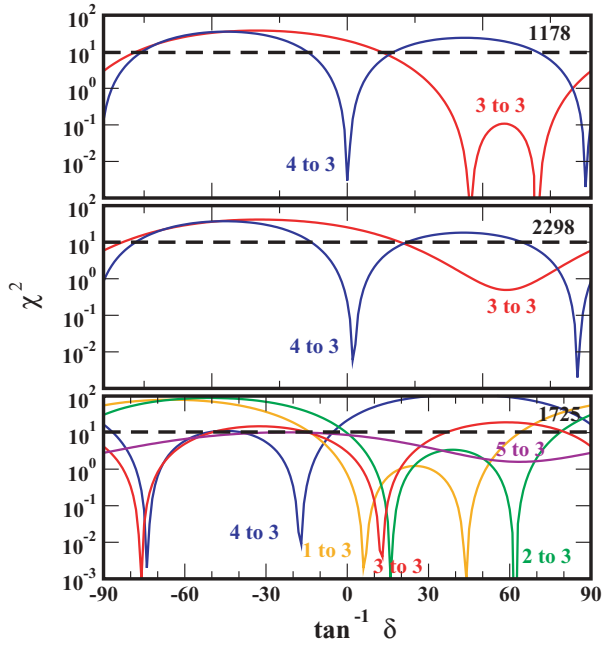

FIG. 14. (Color Online) Goodness of fit χ^2 as a function of mixing ratio δ for the 1178-keV, 2298-keV, and 1725-keV transitions.

4^+ is the most likely spin in the present analysis, followed by 5^+. This assignment is consistent with that from the charge exchange experiment [11].

No angular distributions were reported for the 1562- or 1802-keV states in the $(t,^3\mathrm{He})$ reaction. It was also difficult to obtain reliable γ angular distributions for them in the current work. Both decay to the lowest 2^+ level, which limits their spin parity to a range of 0^+ to 4^+ or 1^- to 3^-. The 2298-keV state was assigned $J = 3$ or 4 in the $(t,^3\mathrm{He})$ reaction [12]. $J = 4$ fits the angular distribution of its ground-state decay with almost zero mixing ratio, whereas $J = 3$ does not give a good fit (Fig. 14). Spin 4 also leads to a good fit at $\delta = 0$ for its 1178-keV decay branch. Spin 3 would imply a large mixing ratio, which is less likely. The fact that it decays only to 3^+ states also favors spin 4. The 2846-keV state is placed based on the observed 1725–1120 and 1725–874–244 cascades.This state is newly observed, so no previous spin information is available. The angular distribution of the 1725-keV decay line is described well by spin hypotheses ranging from 1 to 4 for the 2846-keV level (Fig. 14).

The 2908-keV state was previously assigned spin 4 or 5 with unknown parity. The angular distribution of its 1662-keV decay line strongly favors a spin of 5 (Fig. 15). The angular distribution of its energetically unfavored 608-keV decay branch to another spin 4 state also favors spin 5 and esentially rules out 4 because of the very unlikely large mixing ratio (Fig. 15). The decay of the 3464-keV state to the lowest 4^+ level suggests higher spin and the angular distribution of the 2217-keV γ ray also favors $J = 5$ (Fig. 15).

The 3905-keV state was well described by 5^+ in Ref. [12]. The angular distribution of its 997-keV γ ray is described by a spin sequence of either $5 \rightarrow 4$ or $6 \rightarrow 5$ (Fig. 16) and not by a $\Delta J = 2$ or a $\Delta J = 0$ sequence. Because the 2908-keV state is much more likely to have spin 5, this would lead to an assignment of 6 for the 3905-keV state, in possible disagreement with the $(t,^3\mathrm{He})$ result. However, no calculations for spins higher than 5 are shown in Ref. [12]. The decay of the 3905-keV state only to the lowest spin 5 level and not to any of the lower spin 4 states also makes the hypothesis of spin 6 more likely.

Neither the possible 4293-, nor the 5510- or 6422-keV states, correspond to any previously reported levels. The

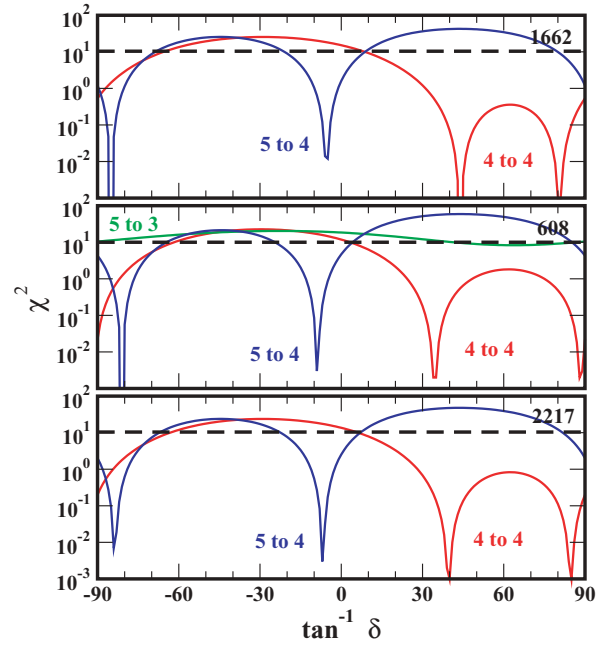

FIG. 15. (Color online) Goodness of fit χ^2 as a function of mixing ratio δ for the 1662-, 608-, and 2217-keV transitions.

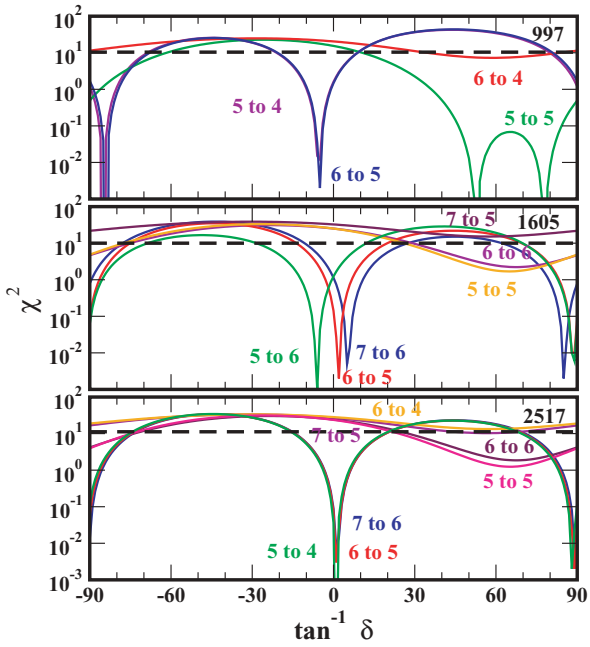

FIG. 16. (Color online) Goodness of fit χ^2 as a function of mixing ratio δ for the 997-, 1605-, and 2517-keV transitions.

angular distribution of the 2517-keV decay of the 6422-keV state is consistent only with $\Delta J = 1$ (Fig. 16).

Note that the 6422-keV state lies about 700 keV above the neutron-decay threshold. Only the angular momentum barrier from a relatively high-spin state would hinder neutron decay so much that γ decay predominates.

B. *sd*-shell model and the positive-parity states

The USD Hamiltonian was adjusted to fit what was known of the structure of *sd*-shell nuclei two decades ago [2,23]. At that time, most of the available structure information was for nuclei in the valley of stability. Since then, a considerable amount of new structure information was measured experimentally for nuclei farther from the valley of stability, especially on the neutron-rich side. Recently, the Hamiltonian was adjusted again to reflect the wealth of new structure learned in the intervening years [8]. The USDA interaction was fitted by allowing 30 linear combinations of the two-body matrix elements to vary from the renormalized G matrix for the *sd* shell, whereas, for the USDB, 56 combinations were allowed to vary. RMS deviations of 170 (126) keV for the 608 energy levels fitted were observed for the USDA (USDB). The present work provides data not used in this fit for comparison with the three calculations in a nucleus with moderate neutron excess.

The *sd*-shell model provides a good comparison for the positive-parity states with predominantly *sd* configurations. These calculations with all three interactions predict the same level ordering up through the lowest 4^+ state. There is also a one-to-one correspondence with the experimental levels (see Fig. 12), although the shell-model energies tend to be somewhat lower. The root-mean-square energy differences are 253, 187, and 191 keV for the USD, USDA, and USDB interactions, respectively, i.e., the USDA and USDB give almost equally good fits to the level energies for the low-lying states, whereas the USD results are a little worse. This provides some support to the conclusion that the newer interactions are better adapted to neutron-rich nuclei.

The electromagnetic transition strengths provide a more detailed comparison between the calculations and experiment. They are shown in Table III. The theoretical branching ratios are based on the calculated $B(M1)$ and $B(E2)$ values (with effective charges of 1.5 and 0.5 for protons and neutrons, respectively) and the experimental transition energies. There is very good agreement in the branching ratios up through the lowest 4^+ state, which gives further confidence in the spin assignments given in Fig. 12.

Focusing on the lowest spin states, only one 1^+ state has been observed above 2 MeV, but all three calculations predict two 1^+ levels at about 2100 and 2500 keV. USD calculations [3] predict log ft values of 3.7, 4.1, and 6.8 for the 493-, 2139-, and 2538-keV levels. These are in good agreement with the experimental values if the 2413-keV state corresponds to the 2139-keV USD prediction. The very weak β branch implied by the large predicted log ft value for the 2538-keV level would explain why it was not observed experimentally. The predicted γ-decay branching ratios for the second theoretical 1^+ state also agree rather well with experiment, keeping in mind that weaker branches would not be observed experimentally.

It is unlikely that the 0^+ states were populated significantly in the $^{14}\mathrm{C} + ^{18}\mathrm{O}$ reaction because even the second 1^+ state was not observed. In the compilation [22], the 991-keV state is shown to decay only to the 1^+ state at 688 keV by a 303-keV γ ray. This would make it a candidate for the first predicted 0^+ state. However, no evidence for a 303-keV γ ray was found in the β-decay or in-beam data. The only published information on the purported 991-keV state is the observation of a ground-state decay [15]. As mentioned, we see no evidence for this transition or state.

The comparison with theory becomes less clear above 1500 keV and spin 1. Based on their energies, the states observed at 1562 and 1802 keV are the best candidates for the predicted 2_2^+ and 2_3^+ levels. However, there is only limited agreement between the observed 100% decay branch of the 1562-keV state to the 244-keV level and the predicted branching ratios of 38% to 57% for the 2_2^+ state. There is essentially no agreement between the observed 100% 1802 $\rightarrow$ 244 keV decay and the 1% to 17% branches calculated for the 2_3^+ state, but partial agreement with the 28% to 51% branches calculated for the 2_4^+ state about 600 keV higher in energy than the 1802-keV level. There is also a much larger variation in the calculated decay branching ratios of the 2^+ states between the three interactions. One possible conclusion is that the 1562- and 1802-keV states both have $J^\pi = 2^+$, but the shell-model calculations are not getting the mixing between the various 2^+ states right. Another possibility is that one or both states are intruders.

The 4_2^+ state is predicted to decay primarily to the lowest two 3^+ levels, in qualitative agreement with the decay pattern observed for the 2298-keV state. However, the calculations predict a stronger branch to the 3_2^+ level, whereas the

TABLE III. A comparison of the experimentally measured branching ratios with those predicted by the *sd*-shell model using the indicated interactions. In some cases more than one possible shell-model state is compared with experiment. The energies shown in the first columns are the experimental ones, whereas the spins and serial numbers shown in the last columns are for the theoretical states.

E_i (keV)	E_f (keV)	Branching ratios (%)				J^π, #
		Exp	USD	USDA	USDB	
688	244	98	100	100	100	1^+, 1
	0	2	0	0	0	
1120	244	69	73	79	71	3^+, 2
	0	31	27	21	29	
1246	0	100	100	100	100	4^+, 1
1562	1120		3	2	3	2^+, 2
	688		2	11	8	
	244	100	38	57	50	
	0		57	30	39	
1802	1120		5	7	9	2^+, 3
	688		35	1	22	
	244	100	17	6	1	
	0		44	86	68	
1802	1687		7	10	3	2^+, 4
	1562		8	3	11	
	1120		9	24	0	
	688		22	8	53	
	244	100	51	28	33	
	0		3	27	0	
2298	1246		0	0	1	4^+, 2
	1120	18	67	60	58	
	244		3	3	3	
	0	82	30	37	38	
2413	688	35	36	44	33	1^+, 2
	244	65	54	44	53	
2846	2298		2	1	1	3^+, 3
	1802		5	3	0	
	1687		1	2	1	
	1562		3	5	3	
	1120	100	19	21	20	
	688		1	1	0	
	244		20	22	18	
	0		46	40	52	
2846	1120	100	75	70	61	4^+,2
	244		5	4	4	
	0		20	26	35	
2908	2846		0	0	0	5^+,1
	2298	57	0	0	12	
	1802		0	4	0	
	1246	43	97	94	86	
	1120		3	3	2	
	0		0	0	0	
3464	2846		8	0	5	5^+,1
	1246	100	87	90	92	
	1120		4	2	3	
	0		1	8	0	
3905	2908	>78	1	9	3	4^+, 3
	2846		6	10	19	
	2298	<22	0	0	0	
	1802		<1	4	6	
	1562		1	22	21	
	1246		1	6	7	
	1120		14	16	13	
	244		1	<1	<1	
	0		75	32	30	
3905	2908	>78	0	0	0	5^+, 2
	2846		0	0	0	
	2298	<22	1	0	0	
	1246		92	90	92	
	1120		1	1	1	
	0		6	9	7	
3905	2908	>78	0	1	1	4^+, 4
	2846		0	0	0	
	2298	<22	0	1	1	
	1246		1	10	15	
	1120		14	23	22	
	0		75	65	61	
3905	2908	>78	36	16	24	6^+, 1
	2298	<22	0	7	1	
	1246		64	77	75	

experimental ratio is reversed. The decay of the 2846-keV state only to the 3_2^+ level agrees significantly better with that predicted for the 4_2^+ state and poorly with that for the 3_3^+ state. The predicted energies of the 4_2^+ states lie roughly midway between 2298 and 2846 keV. Altogether, it appears more likely that the 2846-keV experimentaly state is the predicted 4_2^+ state and the 2298-keV state is not accounted for in the *sd*-shell model.

The 2908-keV state decays with almost equal branches to two spin 4 states below it. A spin of 5 is strongly favored experimentally, but the theoretical 5_1^+ level is predicted to decay almost completely to the 4_1^+ state. Spin 5 was also favored experimentally for the 3464-keV state. Its exclusive decay to the lowest 4^+ state agrees well with the prediction for the 5_1^+ level. Thus the decay patterns strongly suggest that the 3464-keV state is the theoretical 5_1^+ level, but the calculated energies are closer to 2908 keV. However, the energy differences with 3464 keV are not outside the range seen for *sd* calculations, are smaller for the newer interactions, and continue the trend of generally underpredicting the experimental energies.

As discussed, the angular distribution of its decay γ ray favors spin 6 for the 3905-keV state, whereas the $(t,{}^3\mathrm{He})$ angular distribution [12] led to a 5^+ assignment. Although it is close in energy to the predicted 5_2^+ level, the predicted decay pattern is in total disagreement with experiment. There is partial agreement with the predicted decay pattern of the 6_1^+ level, but its energy is almost 2 MeV higher than that of experiment. It is also difficult to find suitable candidates in the *sd* model space for the 5510- and 6422-keV states. Their decay patterns do not resemble those predicted for the 5_3^+, 6_2^+, or 7_1^+ levels.

C. Negative-parity intruder states

Both the absence of good candidates in the sd-shell model for some of the experimental states and the presence of negative-parity states as low as 3500 keV in ^{28}Al [24] strongly suggest that some of the states observed in ^{30}Al have negative parity. In fact, the larger number of neutrons in ^{30}Al is likely to lower the energies for intruder states with configurations involving the $f_{7/2}$ shell.

The good agreement of the states below 1500 keV with the sd-shell model and systematics imply that negative parity is unlikely for for any of these states. As discussed above, the lowest 2^+ states are good candidates for the 1562- and 1802-keV levels based on energy, but the agreement in decay patterns is not very good. Because these two states decay to the 2^+ level, possible negative parities are 1^-, 2^-, and 3^-. The lowest 3^- state lies at 3591 keV in ^{28}Al. It is somewhat doubtful that this state would drop 1.8 to 2 MeV with the addition of two neutrons, and the absence of any decays to the 3^+ ground state or any decays to the 1562- and 1802-keV states from higher-lying states with higher spins make spin 3 unlikely for either state. Thus 2^+ remains most likely for these two states, but 1^- or 2^- cannot be ruled out.

Spin 4 was assigned to the 2298-keV state, but no good positive-parity candidate was identified. It appears likely that this may be a 4^- state corresponding to the lowest negative-parity state in ^{28}Al at 3465 keV. That would imply a rather reasonable drop in energy of 1167 keV. The angular distribution of its 1178-keV line implies a zero mixing ratio that is consistent with pure $E1$ decay (Fig. 14).

The 2908-keV state is a good candidate for 5^- and would imply a similar drop in energy with the corresponding state in ^{28}Al. This interpretation would explain why a low-energy 608-keV transition can compete favorably with one of 1662 keV—an observation not understandable for a 5^+ state in the sd-shell model. It is a case of a low-energy $M1$ transition competing with a higher-energy $E1$. In fact, the assignment of 4^- to the 2298-keV state requires negative parity for the 2908-keV state because a low-energy $E1$ could not compete with a much higher energy $M1$. Also, the angular distribution of the 1662-keV decay is consistent with pure $E1$ decay, as is required for a 5^- assignment.

The 3905-keV state is a likely candidate for 6^-. Its decay to only higher spin states implies moderately high spin, but its decay pattern does not fit any of the reasonable positive-parity candidates. The angular distribution of its 997-keV decay line fits $6^- \rightarrow 5^-$ with a small mixing ratio (Fig. 16). The possible $E2$ branch to the 2298-keV 4^- state is also consistent. Although the angular distribution of the 1605- to 1607-keV possible doublet shows predominantly $\Delta I = 1$ character, a weaker unresolved $E2$ line is not ruled out. The 5510- and 6422-keV states are likely to be 7^- because their decay angular distributions have predominantly $\Delta I = 1$ character.

To better explore the relation between the isotopes, the level schemes of ^{28,30}Al are compared in Fig. 17. There are some similarities in the positive-parity states, and the significant differences reflect the changing number of neutrons in the sd shell. However, Fig. 17 suggests that the main effect of the extra two neutrons on the negative-parity states is just a lowering of all the $\pi = -$ levels. To make this clearer, the

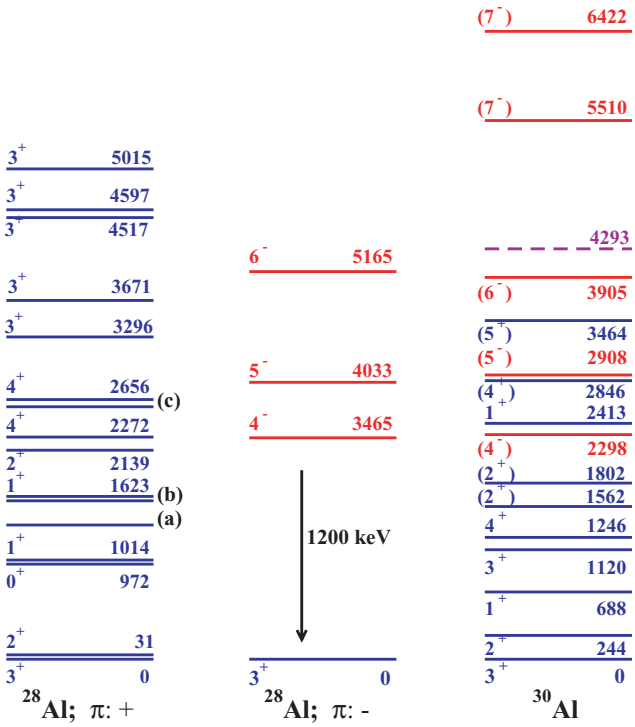

FIG. 17. (Color online) A comparison of the ^{28,30}Al level schemes. The vertical positions of the negative-parity states in ^{28}Al have been shifted down by 1200 keV, as discussed in the text. Levels not labeled in the figure for lack of space are (a) 1373 keV 1^+, (b) 1620 keV 1^+, and (c) 2582 keV 5^+.

$\pi = -$ levels in ^{28}Al have been shifted down by 1200 keV in the figure. The proposed lowest 4^-, 5^-, and 6^- states in ^{30}Al agree rather well in energy with their counterparts in ^{28}Al after the shift. Presumably this shift reflects the lower energy cost of promoting a $d_{3/2}$ neutron up to the $f_{7/2}$ shell compared to that for an $s_{1/2}$ neutron in ^{28}Al. Additional evidence comes from a comparison of the decay branches of the lowest negative-parity levels, shown in Table IV. There is a considerable similarity in the decay patterns for the two isotopes in spite of the ~1.2 MeV energy difference. These comparisons cannot be extended to the 7^- states, because none are known in ^{28}Al.

Further evidence of a systematic shift in intruder energies with changing N and Z comes from a comparison of the lowest 4^- levels in the even Al ($Z = 13$) [25] and P ($Z = 15$) [26] shown in Fig. 18. The decrease in excitation energy of intruder configurations with both increasing N and decreasing Z is typical of "island of inversion" effects where the $N = 20$ shell gap decreases with increasing neutron excess. The almost identical energies for ^{28}Al-^{30}P and ^{30}Al-^{32}P (within 21 and 7 keV, respectively) suggest that the position of the intruder state is dependent almost entirely on N-Z.

Preparation of this graph suggested a re-examination of ^{26}Na that has been studied with essentially the same combination of reactions. The state at 2284-keV decays exclusively to the 3^+ ground state [27], which would be consistent with 4^-. It was assigned 5^+ in the analysis of a $(t,{}^3\mathrm{He})$ reaction [12]. However, a portion of that angular distribution was blocked by a contaminant, and the authors stated that the 4^- and 5^-

TABLE IV. A comparison of the negative-parity decays for ^{28}Al and ^{30}Al. All energies are in keV.

^{28}Al			^{30}Al		
$E_i(J^\pi, \#)$	$E_f(J^\pi, \#)$	Branch (%)	$E_i(J^\pi, \#)$	$E_f(J^\pi, \#)$	Branch (%)
3465(4^-, 1)	2272(4^+, 1)	7		2298(4^-, 1)	
	1014(3^+, 2)	5		1120(3^+, 2)	7
	0(3^+, 1)	88		0(3^+, 1)	93
4033(5^-, 1)	3466(4^-, 1)	51	2908(5^-, 1)	2298(4^-, 1)	79
	2272(4^+, 1)	49		1246(4^+, 1)	21
5165(6^-, 1)	4034(5^-, 1)	100	3905(6^-, 1)	2908(5^-, 1)	71
				2298(4^-, 1)	29

angular distributions are very similar in shape to the 4^+ and 5^+ ones. Thus the 2284-keV state is at least a candidate for 4^-. This possibility is included in Fig. 18, where it fits in very nicely, differing from the corresponding level in ^{30}Al by 16 keV.

D. WBP interaction and the negative-parity states

An extended shell-model space including the *sd* and *pf* shells was used to calculate the expected positions of $1\hbar\omega$ intruder states with the WBP interaction [28]. Although it might be expected to give a good representation of the relative spacing of the $\pi = -$ states, their position relative to the $\pi = +$ levels may not be well predicted because of model limitations. Therefore we have shifted the predicted $\pi = -$ states down by about 1 MeV to force agreement with the lowest 4^- experimental state. These results for ^{30}Al for the $\pi = -$ states are shown in the column labeled "WBP" in Fig. 12. For simplicity, only the yrast and near yrast states are shown, because the in-beam experiment populated only such states. By construction the WBP interaction was designed to reproduce the USD predictions for the $\pi = +$ *sd* states, so its predictions for the $\pi = +$ levels are identical to those in the column labeled "USD." The agreement with the lowest 5^-, 6^-, and 7^- states is remarkably good, and the second 7^- level differs by 300 keV.

The WBP calculations for the lowest 4^- states in the neighboring Al isotopes are shown as a dashed line in Fig. 18. The calculated results were also shifted down by the same 1 MeV, as adjusted in ^{30}Al, so only the values for ^{28}Al and ^{32}Al are predictions. Not only is the decreasing trend with increasing N reproduced well, the value for ^{32}Al agrees perfectly and that for ^{28}Al, reasonably well.

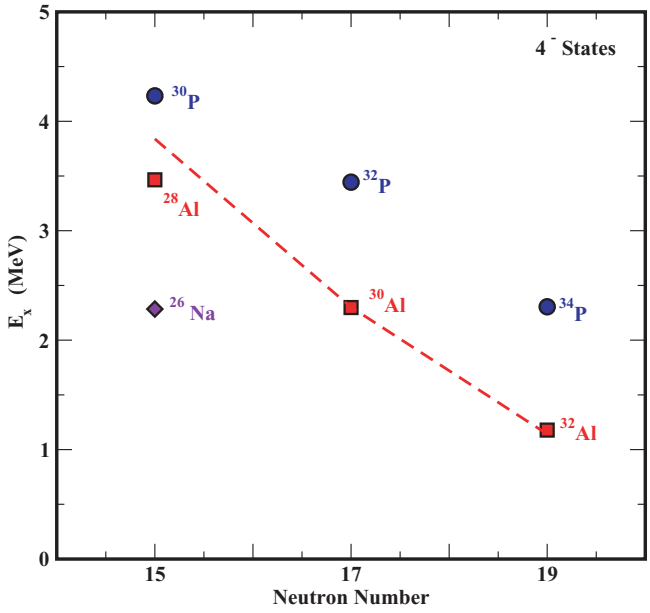

FIG. 18. (Color online) Position of the lowest 4^- states as a function of neutron number in the $Z = 13$ Al and $Z = 15$ P isotopes. The dashed line represents WBP predictions for the Al isotopes adjusted down by about 1 MeV as discussed in the text. Note that some of these spin-parity assignments are tentative.

V. SUMMARY

Complementary techniques were used to study the structure of ^{30}Al. The low-spin states were investigated following the β decay of ^{30}Mg, which was produced in the fragmentation of ^{48}Ca at the MSU NSCL. The A and Z identified fragments from the A1900 separator were correlated with subsequent β and γ decays in a DSSD. The higher-spin states were investigated at FSU in the reaction of ^{14}C on ^{18}O by observing the p-γ, p-γ-γ, d-γ, and d-γ-γ coincidences.

The β-decay experiment has located a new state at 2413 keV, given further confidence to the entire β-decay level scheme through β-γ-γ coincidences, provided firm spin assignments of 1^+ to the 688- and 2413-keV states, and determined a more accurate half-life for the ground state of ^{30}Mg. The in-beam experiment at FSU has revealed for the first time the γ decay scheme of many higher-spin states. A dozen states were seen that correspond well in energy with those previously reported in the charge exchange reaction. Four more states were seen in the present work that do not have counterparts from previous work. The γ decay modes and angular distributions provide spin assignments and restrictions for these states.

The excitation energies and decay branching ratios of the states observed in ^{30}Al were compared with the predictions of the *sd* shell model using both the older USD and newer USDA and USDB interactions. Ten states agree relatively well with the calculations and thus appear to involve pure or nearly pure *sd* structure. The root-mean-square deviations in energy between experiment and theory for these states are 265, 175, and 173 keV, respectively. Clearly USDA and USDB provide better agreement with experiment, with no significant difference between them.

Five states whose decay patterns and energies do not agree well with the *sd* calculations are very likely negative-parity states with configurations involving one $f_{7/2}$ neutron. The proposed 4^-, 5^-, and 6^- levels agree rather well in energy with the lowest corresponding states in ^{28}Al after the ^{28}Al states are shifted down by 1200 keV. The two highest states seen appear to be 7^- states but no 7^- states are known in ^{28}Al for comparison. Calculations using the WBP interaction agree well with the negative-parity states. The decreasing energy of the intruder states with increasing neutron number fits well with the systematics of the even A, Al, and P isotopes. There is also a systematic decrease with decreasing proton number. This variation with N and Z is characteristic of the island of inversion, i.e., the effects of pf intruder configurations increase not only with increasing N as it approaches $N = 20$ but also decreasing Z. A very interesting relation seen is that the energy of the lowest 4^- level is almost identical for ^{28}Al and ^{32}P as well as for ^{30}Al and ^{34}P. In these cases, the 4^- energy depends only on N-Z. The relation also suggests an reassignment of 4^- to the 2284-keV level in ^{26}Na. If confirmed, this would demonstrate a sequence of three isotopes with constant N-Z ($= 4$) and almost constant 4^- energy.

ACKNOWLEDGMENTS

This work was supported in part by the US National Science Foundation under grants PHY-01-39950, PHY-01-10253, and PHY-04-56463. We thank Y. Utsuno for valuable discussions, the NSCL staff for smooth running of the accelerator, and Powell Barber for fabrication of the ^{18}O target.

[1] I. Talmi and I. Unna, Phys. Rev. Lett. **4**, 469 (1960).
[2] B. H. Wildenthal, Prog. Part. Nucl. Phys. **11**, 5 (1984).
[3] B. H. Wildenthal, M. S. Curtin, and B. A. Brown, Phys. Rev. C **28**, 1343 (1983).
[4] C. Thibault, R. Klapisch, C. Rigaud, A. M. Poskanzer, R. Prieels, L. Lessard, and W. Reisdorf, Phys. Rev. C **12**, 644 (1975).
[5] Vandana Tripathi, S. L. Tabor, P. F. Mantica, C. R. Hoffman, M. Wiedeking, A. D. Davies, S. N. Liddick, W. F. Mueller, T. Otsuka, A. Stolz, B. E. Tomlin, Y. Utsuno, and A. Volya, Phys. Rev. Lett. **94**, 162501 (2005).
[6] Vandana Tripathi, S. L. Tabor, C. R. Hoffman, M. Wiedeking, A. Volya, P. F. Mantica, A. D. Davies, S. N. Liddick, W. F. Mueller, A. Stolz, B. E. Tomlin, T. Otsuka, and Y. Utsuno, Phys. Rev. C **73**, 054303 (2006).
[7] Vandana Tripathi, S. L. Tabor, P. F. Mantica, Y. Utsuno, P. Bender, J. Cook, C. R. Hoffman, Sangjin Lee, T. Otsuka, J. Pereira, M. Perry, K. Pepper, J. Pinter, J. Stoker, A. Volya, and D. Weisshaar, Phys. Rev. C **76**, 021301(R) (2007).
[8] B. A. Brown and W. A. Richter, Phys. Rev. C **74**, 034315 (2006).
[9] Yutaka Utsuno, Takaharu Otsuka, Thomas Glasmacher, Takahiro Mizusaki, and Michio Honma, Phys. Rev. C **70**, 044307 (2004).
[10] Ajzenberg-Selove and G. Igo, Phys. Rev. C **188**, 1813 (1969).
[11] K. I. Pearce, N. M. Clarke, R. J. Griffiths, P. J. Simmonds, A. C. Dodd, D. Barker, J. B. A England, M. C. Mannion, and C. A. Ogilvie, Phys. Rev. C **35**, 1617 (1987).
[12] N. M. Clarke and K. I. Pearce, J. Phys. G: Nucl. Part. Phys. **15**, L249 (1989).
[13] C. Detraz, D. Guillemaud, G. Huber, R. Klapisch, M. Langevin, F. Naulin, C. Thibault, L. C. Carraz, and F. Touchard, Phys. Rev. C **19**, 164 (1979).
[14] D. Guillemaud-Mueller, C. Detraz, M. Langevin, F. Naulin, M. De Saint-Simon, C. Thibault, F. Touchard, and M. Epherre, Nucl. Phys. A **426**, 37 (1984).
[15] R. L. Kozub, C. B. Chitwood, D. J. Fields, C. J. Lister, J. W. Olness, and E. K. Warburton, Phys. Rev. C **28**, 2343 (1983).
[16] J. I. Prisciandaro, A. C. Morton, and P. F. Mantica, Nucl. Instrum. Methods Phys. Res. **505**, 140 (2003).
[17] S. W. Padgett, Vandana Tripathi, S. L. Tabor, P. F. Mantica, C. R. Hoffman, M. Wiedeking, A. D. Davies, S. N. Liddick, W. F. Mueller, A. Stolz, and B. E. Tomlin, Phys. Rev. C **72**, 064330 (2005).
[18] W. F. Mueller, J. A. Church, T. Glasmacher, D. Gutknecht, G. Hackman, P. G. Hansen, Z. Hu, K. L. Miller, and P. Quirin, Nucl. Instrum. Methods Phys. Res. **466**, 492 (2001).
[19] J. Pavan, Ph. D. thesis, Florida State University, 2003.
[20] J. P. Dufour, R. Delmoral, A. Fleury, F. Hubert, D. Jean, M. S. Provikoff, H. Delagrange, H. Geissel, and K. H. Schmidt, Z. Phys. A **324**, 487 (1986).
[21] P. M. Endt and R. B. Firestone, Nucl. Phys. **A633**, 1 (1998).
[22] G. Audi, A. H. Wapstra, and C. Thibault, Nucl. Phys. **A792**, 1 (2003).
[23] B. A. Brown and B. H. Wildenthal, Annu. Rev. Nucl. Part. Sci. **38**, 29 (1988).
[24] http://www.nndc.bnl.gov/ensdf/.
[25] B. Fornal, R. Broda, W. Królas, T. Pawlat, J. Wrzesinski, D. Bazzacco, D. Fabris, S. Lunardi, C. Rossi Alvarez, G. Viesti, G. de Angelis, M. Cinausero, D. R. Napoli, and Z. W. Grabowski, Phys. Rev. C **55**, 762 (1997).
[26] J. Ollier, R. Chapman, X. Liang, M. Labiche, K.-M. Spohr, M. Davison, G. de Angelis, M. Axiotis, T. Kröll, D. R. Napoli, T. Martinez, D. Bazzacco, E. Farnea, S. Lunardi, A. G. Smith, and F. Haas, Phys. Rev. C **71**, 034316 (2005).
[27] Sangjin Lee, S. L. Tabor, T. Baldwin, D. B. Campbell, I. Calderin, C. Chandler, M. W. Cooper, C. R. Hoffman, K. W. Kemper, J. Pavan, A. Pipidis, M. A. Riley, and M. Wiedeking, Phys. Rev. C **73**, 044321 (2006).
[28] E. K. Warburton and B. A. Brown, Phys. Rev. C **46**, 923 (1992).